Journal of Computational Physics 297 (2015) 295–315

Contents lists available at ScienceDirect

Journal of Computational Physics

www.elsevier.com/locate/jcp

Compact high order schemes with gradient-direction derivatives for absorbing boundary conditions

Dan Gordon [a,*], Rachel Gordon [b], Eli Turkel [c]

[a] Department of Computer Science, University of Haifa, Haifa 3498838, Israel
[b] Department of Aerospace Engineering, the Technion–Israel Inst. of Technology, Haifa 32000, Israel
[c] School of Mathematical Sciences, Tel Aviv University, Tel Aviv 69978, Israel

ARTICLE INFO

Article history:
Received 18 November 2014
Received in revised form 20 May 2015
Accepted 21 May 2015
Available online 27 May 2015

Keywords:
Absorbing boundary conditions
Compact schemes
Geophysics
Gradient method
Helmholtz equation
High order accuracy
Wavefront direction

ABSTRACT

We consider several compact high order absorbing boundary conditions (ABCs) for the Helmholtz equation in three dimensions. A technique called "the gradient method" (GM) for ABCs is also introduced and combined with the high order ABCs. GM is based on the principle of using directional derivatives in the direction of the wavefront propagation. The new ABCs are used together with the recently introduced compact sixth order finite difference scheme for variable wave numbers. Experiments on problems with known analytic solutions produced very accurate results, demonstrating the efficacy of the high order schemes, particularly when combined with GM. The new ABCs are then applied to the SEG/EAGE Salt model, showing the advantages of the new schemes.

1. Introduction

We consider compact high order absorbing boundary conditions (ABCs) for the Helmholtz equation in a finite domain D:

$$\Delta u + k^2 u = F, \tag{1}$$

where $k(x, y, z)$ is the wavenumber, and $F(x, y, z)$ is typically the displacement at a point or region of D. We consider various high order absorbing boundary conditions (ABCs) and introduce a new technique called "the gradient method" (GM) as a new approach to ABCs for the Helmholtz equation, and possibly, for other partial differential equations of physics. GM is based on the principle of using directional derivatives of u in the direction of the wavefront propagation, i.e., the direction of ∇u (the gradient of u). In many important cases the direction of the wavefront propagation is known a priori, e.g., when there is a single point source or in the case of plane waves. In such cases, GM can be used to derive a linear system. When ∇u is not known a priori, the use of GM leads to a nonlinear problem which requires nonlinear solution methods.

In many applications F is a function of small finite support. For example, in geophysics, a typical method of reconstructing the structure of some volume of the earth consists of creating an impact at some point in the volume, with many detectors measuring the resulting reverberations. This is repeated at many impact points. One important reconstruction method, known as "full waveform inversion" (FWI) handles the reconstruction problem in the frequency domain, and it involves the repeated numerical solution of the Helmholtz equation; see Virieux and Operto [39]. In this setup, the function F in Eq. (1) describes the source of impact, and it has a small support.

* Corresponding author.
E-mail addresses: gordon@cs.haifa.ac.il (D. Gordon), rgordon@tx.technion.ac.il (R. Gordon), turkel@post.tau.ac.il (E. Turkel).

http://dx.doi.org/10.1016/j.jcp.2015.05.027
0021-9991/

Three major issues affect the accuracy of the solution obtained by any numerical method: the accuracy of the interior scheme used, the accuracy of solver, and the absorbing boundary conditions. We shall use the recently introduced sixth order accurate finite difference scheme for variable k [35]. The ability to handle variable values of k is essential for many applications in which the domain is heterogeneous. As to the solver, we use the CARP-CG algorithm [16], which was found to be very useful for solving the Helmholtz equation at high frequencies, including applications with high order finite difference schemes. See [18] for another preconditioned Krylov subspace method.

We will be concerned with the third issue mentioned above: high-accuracy ABCs. To this end, we will consider two complementary approaches: (1) high order schemes for ABCs, and (2) the gradient method (GM), whereby directional derivatives of u that appear in the ABC are taken in the direction of ∇u. The motivation for GM stems from the Sommerfeld radiation condition [32, §28] which uses directional derivatives in the radial direction, which is also the direction of ∇u when there is a single point source. Many ABCs that are based on the Sommerfeld radiation condition, such as the Engquist–Majda ABCs [11], use derivatives in the direction normal to the boundary. This normal direction can deviate significantly from the radial direction that appears in Sommerfeld's condition. Furthermore, the normal direction is discontinuous at the corners of two dimensional rectangular domains and edges of three dimensional box-shaped domains. Some ABCs apply certain corrections to ameliorate this problem, e.g., Higdon's method [20], which generalizes the Engquist–Majda ABCs. For a review of ABCs, see [12]. We reiterate that if we know, in advance, that the solution behaves radially, e.g. a point source, then we can take, in advance, the gradient direction as the radial direction.

We consider high order schemes for two classes of ABCs: the Engquist–Majda ABCs [11] (abbreviated EM), and the Bayliss, Gunzburger and Turkel ABCs [5] (abbreviated BGT). In addition to high order accuracy it is useful to consider compact stencils ($3 \times 3 \times 3$ in 3D). This has several advantages. Foremost, is that no non-physical boundary conditions need to be considered. In addition, this reduces the bandwidth of the matrix to be inverted. Another practical advantage is that huge 3D domains require parallel solvers. Compact schemes lend themselves more easily to parallel domain decomposition techniques, such as the CARP-CG algorithm used in this work. The application of GM to the EM ABCs consists of replacing the normal derivatives of EM with directional derivatives in the direction of ∇u. This operation might appear to be counter-intuitive, but as mentioned above, it is in keeping Sommerfeld's radiation condition. Furthermore, our experiments show that the application GM to EM produces ABCs that are much more accurate than EM.

The BGT ABCs were originally developed for scattering about bodies with an incident plane wave. The outer artificial surface was assumed to a circular domain in two dimensions or a spherical domain in three dimensions. So these ABCs used radial derivatives of u (whose direction is also normal to the boundary). The application of GM to the BGT ABCs means that they can be used unchanged in any convex domain, and with a source at any interior point, even when the radial direction does not coincide with the normal direction at the boundaries. Kriegsmann, Taflove and Umashankar [22] considered an extension of BGT to be placed directly on the scatterer, called "on surface radiation condition" (OSRC). To accomplish this, they replaced the radial derivatives by normal derivatives to the scatterer, and the inverse radius by the radius of curvature of the scatterer. Medvinsky, Turkel and U. Hetmaniuk constructed an extension of BGT to an outer surface that is an ellipse based on expansions in Mathieu functions. See [24] for details and further citations. Zarmi and Turkel [41] discuss a more general approach to ABCs in various coordinate systems.

Although GM is applied in this work only to ABCs for the Helmholtz equation, it might also be applicable to other equations which require ABCs, such as Euler's equation, Schrödinger's equation, Maxwell equations, and the 3D elastic wave equation in the frequency domain (which is also used in seismic applications).

A widely used method for ABCs is that of the perfectly matched layer (PML) [6,7], which requires the addition of several layers of extra grid points around the domain. The main disadvantage of this approach is that significant extra memory is required, not to mention the extra computation time imposed by the additional equations. For example, if the original mesh is $100 \times 100 \times 100$ and a PML of 10 points is introduced on each side, then the new mesh is of size 120^3, and this increases the storage by about 73%. Even with a large mesh of $500 \times 500 \times 500$ (i.e. 125 million nodes) a 10 point PML in all directions adds about 12.5% to the storage. As we shall see, the high order ABCs (with just one extra layer), combined with GM, produce very accurate results which are sufficient for all practical purposes.

The rest of the paper is organized as follows. Section 2 describes the EM and BGT ABCs and Section 3 develops the high order approximations to these ABCs. Section 4 describes GM, and Section 5 explains some implementation details for the experiments. Section 6 presents experimental results on a model with known analytic solutions, and Section 7 shows the results obtained with the SEG/EAGE Salt model. We conclude with Section 8. In Appendix A we present some mathematical properties of the ABCs and analyze the self-adjointness of these operators at both the continuous and discrete levels. Appendix B contains the explicit stencils of two of our ABC schemes.

2. The EM and BGT ABCs

2.1. The Sommerfeld radiation condition

Throughout the following, we shall use the boldface letters $\boldsymbol{r}$, $\boldsymbol{n}$ and $\boldsymbol{g}$ to denote unit vectors in the radial direction, normal (to the boundary) direction, and the gradient direction of u, respectively.

Sommerfeld [32, §28] shows that the following "radiation condition" is sufficient for the well-posedness of the Helmholtz equation (1) in an exterior unbounded region when the RHS function $F(x, y, z)$ has a compact support.

$$\lim_{r\to\infty} r\left(\frac{\partial u}{\partial \boldsymbol{r}} - iku\right) = 0, \tag{2}$$

where r is the distance from a point to the source and $\frac{\partial u}{\partial \boldsymbol{r}}$ denotes the directional derivative of u in the radial direction. ABCs that are based on this radiation condition strive to mimic it on the boundaries of the domain. The following subsections present two well-known examples of such ABCs.

2.2. The Engquist–Majda ABCs

Engquist and Majda [11] proposed a sequence of boundary conditions. We will refer to these conditions as EMm. We will denote by EM the class of all EMm methods, $m \geq 1$. Engquist and Majda constructed these ABCs by splitting the wave operator into right and left moving waves and eliminating the incoming wave. This results in pseudo-differential operators which were then approximated by differential operators.

Higdon [20] extended the EM method by selecting several predetermined directions, not necessarily all normal to the outer boundary, along which there will be no reflection. For all other in-between directions, there will be some reflection (in Higdon's method) back to the computational domain. Although we shall consider only the original EM ABCs and not Higdon's extensions, we shall use Higdon's approach that constructs the high-order operators as products of the EM1 operator.

EM1 is the following ABC:

$$\text{EM1:}\quad u_{\boldsymbol{n}} - iku = 0, \tag{3}$$

where $u_{\boldsymbol{n}} = \partial u/\partial \boldsymbol{n}$ is the directional derivative of u in the direction of $\boldsymbol{n}$.

The second order EM ABC, EM2, is given by

$$\text{EM2:}\quad (\frac{\partial}{\partial \boldsymbol{n}} - ik)^2 u = u_{\boldsymbol{nn}} - 2iku_{\boldsymbol{n}} - k^2 u = 0. \tag{4}$$

There are two problems with the EM approach when the domain is rectangular and the source is a point. One problem is that almost everywhere, $u_{\boldsymbol{n}} \neq u_{\boldsymbol{r}}$, i.e., the normal derivative differs from the radial derivative in Sommerfeld's radiation condition. The difference between them can be arbitrarily close to $\pi/2$. Another problem is that $u_{\boldsymbol{n}}$ and $u_{\boldsymbol{nn}}$ are not continuous at the corners of the domain. The only case when these problems disappear is when the domain is circular (or spherical in 3D) and there is a point source at the center. In the results section we shall see the computational significance of these problems: the error in the neighborhood of the corners is much larger than the overall error.

2.3. The Bayliss–Gunzburger–Turkel ABCs

A different approach from the EM operators is presented by Bayliss, Gunzburger and Turkel [5]. Assuming a spherical domain with a scatterer (or compact source) at the center, then in three dimensions there is a sequence of functions $f_0, f_1, \ldots$ such that the solution u is given by the following convergent series

$$u(r, \theta, \phi) = \frac{e^{ikr}}{kr} \sum_{j=0}^{\infty} \frac{f_j(\theta, \phi)}{(kr)^j}, \tag{5}$$

where r, θ, ϕ are the standard spherical coordinates. They constructed a series of ABCs $B_m = 0$ in the inverse radius that match the first m terms of this series. We shall use the abbreviation BGTm to denote the mth order ABC of [5], and BGT to refer to the entire class of BGTm, for $m \geq 1$. For 3D, BGT1 is defined as

$$\text{BGT1:}\quad B_1 u \equiv \frac{\partial u}{\partial \boldsymbol{r}} + \left(\frac{1}{r} - ik\right) u = 0, \tag{6}$$

where $\frac{\partial u}{\partial \boldsymbol{r}} = u_{\boldsymbol{r}}$ is the derivative of u in the radial direction and r is the distance between the point on the boundary and the source. If the point source is at the center of a spherical domain, then on the boundary, we also have $u_{\boldsymbol{n}} = u_{\boldsymbol{r}}$.

For $m \geq 2$, $B_m u$ is defined as

$$B_m u \equiv \left(\frac{\partial}{\partial \boldsymbol{r}} + \frac{2m-1}{r} - ik\right)\left(B_{m-1} u\right) = 0.$$

Hence, any function which satisfies $B_{m-1} u = 0$ also satisfies $B_m u = 0$. B_2 is given by:

$$\text{BGT2:}\quad B_2 u \equiv u_{\boldsymbol{rr}} + \alpha(r) u_{\boldsymbol{r}} + \beta(r) u = 0, \tag{7}$$

where

$$\alpha(r) = \left(\frac{4}{r} - 2ik\right) \quad \text{and} \quad \beta(r) = \left(\frac{2}{r^2} - k^2 - \frac{4ik}{r}\right).$$

If needed, $u_{\boldsymbol{rr}}$ can be eliminated in terms of the first order tangential derivatives by using the Helmholtz equation. This is useful for linear finite elements where a second derivative cannot be used. For the finite difference method this is not needed and so we shall only consider (7). $u_{\boldsymbol{r}}$ and $u_{\boldsymbol{rr}}$ can also be expressed in terms of Cartesian coordinates – see Equations (31) and (32).

When the source is a Dirac delta function, then the solution to the Helmholtz equation is Green's function. For 3D, $G(r) = \frac{e^{ikr}}{4\pi r}$ (see also Section 6.1). BGT1 and hence all BGTm are exact for G. G_r satisfies BGT2 but not BGT1. Since $G_x = G_r r_x$ and $r_x = \frac{r}{x}$ is independent of r, G_x also satisfies BGT2. Naturally, a discretization of BGT will destroy the exactness, and so BGT1 and BGT2 will be accurate only to the order of the discretization error. By straightforward differentiation, all Cartesian derivatives of G satisfy the homogeneous Helmholtz equation. However, radial derivatives of G do not satisfy the homogeneous Helmholtz equation.

3. Compact high order approximations to the ABCs

Since the domain is infinite in some directions we need to truncate the domain for computational purposes. Along these outer artificial surfaces we impose an absorbing boundary condition in order to reduce reflections from the artificial surface into the physical domain. The error introduced by the ABC has two distinct sources. One is the accuracy of the ABC on the continuous level. As these ABCs need to be discretized there is an additional error introduced by the discretization. The higher order ABCs involve higher order derivatives. Hence, in general, one can only discretize them on a compact stencil with a lower order accurate discretization. We shall compare high order ABCs with a low order discretization with a lower order ABC but a higher order accurate discretization. In this section we will assume that k in the Helmholtz equation is constant, and $F = 0$ in the neighborhood of the outer artificial surface.

3.1. High order approximation to derivatives

Using a Taylor series expansion we have (ignore j and k indices)

$$\delta_x u \equiv \frac{u_{i+1} - u_{i-1}}{2h} = u_x + \frac{h^2}{6}u_{xxx} + O(h^4),$$
$$\delta_{xx} u \equiv \frac{u_{i+1} - 2u_i + u_{i-1}}{h^2} = u_{xx} + \frac{h^2}{12}u_{xxxx} + O(h^4)$$

or

$$u_x = \frac{u_{i+1} - u_{i-1}}{2h} - \frac{h^2}{6}u_{xxx} + O(h^4),$$
$$u_{xx} = \frac{u_{i+1} - 2u_i + u_{i-1}}{h^2} - \frac{h^2}{12}u_{xxxx} + O(h^4). \tag{8}$$

Differentiating the Helmholtz equation (1) we get

$$u_{xxx} = -\left(u_{xyy} + u_{xzz} + k^2 u_x\right) + F_x,$$
$$u_{xxxx} = -\left(u_{xxyy} + u_{xxzz} + k^2 u_{xx}\right) + F_{xx}. \tag{9}$$

Substituting (9) into (8) we get

$$u_x = \delta_x u + \frac{h^2}{6}\left(u_{xyy} + u_{xzz} + k^2 u_x\right) - \frac{h^2}{6}F_x + O(h^4),$$
$$u_{xx} = \delta_{xx} u + \frac{h^2}{12}\left(u_{xxyy} + u_{xxzz} + k^2 u_{xx}\right) - \frac{h^2}{12}F_{xx} + O(h^4).$$

Replacing the derivatives by central differences we get

$$u_x = \left(1 + \frac{k^2 h^2}{6}\right)\delta_x u + \frac{h^2}{6}\left(\delta_{xyy} u + \delta_{xzz} u\right) - \frac{h^2}{6}F_x + O(h^4), \tag{10a}$$
$$u_{xx} = \left(1 + \frac{k^2 h^2}{12}\right)\delta_{xx} u + \frac{h^2}{12}\left(\delta_{xxyy} u + \delta_{xxzz} u\right) - \frac{h^2}{12}F_{xx} + O(h^4). \tag{10b}$$

We next consider a typical mixed derivative. By Taylor series

$$\delta_{xy}u = u_{xy} + \frac{h^2}{6}(u_{xxxy} + u_{xyyy}) + O(h^4). \tag{11}$$

Differentiating (1) with respect to x and y gives

$$u_{xxxy} + u_{xyyy} = -\left(u_{xyzz} + k^2 u_{xy}\right).$$

Substituting into (11) gives:

$$u_{xy} = (1 + \frac{k^2h^2}{6})\delta_{xy}u + \frac{h^2}{6}\delta_{xyzz}u + O(h^4). \tag{12}$$

3.2. EM1 with pseudo-6th order accuracy

We consider the first order generalized EM ABC:

$$u_x + i\beta u = 0 \tag{13}$$

(for the EM ABC, $\beta = k$).

We wish to construct an approximation to the boundary conditions that maintains the high order accuracy. By Taylor series we have:

$$\frac{u_{N+1} - u_{N-1}}{2h} = \frac{\partial u}{\partial x} + \frac{h^2}{6}\frac{\partial^3 u}{\partial x^3} + \frac{h^4}{120}\frac{\partial^5 u}{\partial x^5} + O(h^6), \tag{14}$$

where the $N+1$-th grid point lies outside the computational domain and so is a virtual point.

To get the higher order x derivatives on a compact stencil we differentiate (13) several times in the x direction. This yields (see [9]):

$$0 = \frac{\partial u}{\partial x} + i\beta u = \frac{u_{N+1} + 2i\beta h\left(1 - \frac{\beta^2h^2}{6} + \frac{\beta^4h^4}{120}\right)u_N - u_{N-1}}{2h} + O(h^6). \tag{15}$$

This is combined with the discretization of the Helmholtz equation at the N-th grid point to eliminate the u_{N+1} term.

We stress that in general this is illegal! Given a boundary condition it is not legitimate to differentiate it in a direction perpendicular to the surface. Hence, the numerical absorbing boundary condition which we derive is correct only if the solution behaves like $u(x, y, z) = e^{i\beta x}f(y, z)$ to at least to fourth order accuracy, in a layer about the absorbing boundary, x given. In the result section we shall check if this "illegal" ABC is nevertheless still accurate.

3.3. EM1 with 6th order accuracy

We again consider the first order EM ABC given by (13). To derive a true sixth order approximation we first consider a Neumann boundary condition $u_x = g(y, z)$ at $x = 1$ which is constructed by using the Helmholtz equation to reduce high order derivatives to lower order derivatives. In [35] we constructed a compact sixth order approximation to a Neumann boundary condition for the Helmholtz equation even with a variable wavenumber k. Let δ_x and δ_{xx} be the standard central first and second differences in the x direction.

We assume that k is constant and the forcing function F is zero in the vicinity of the farfield boundary. Then the boundary condition in [35] reduces to

$$\begin{aligned}\delta_x u = {} & g - \frac{h^2}{6}\left(g_{yy} + g_{zz} + k^2 g\right) \\ & + \frac{h^4}{120}\left[g_{yyyy} + 2g_{yyzz} + g_{zzzz} + 2k^2\left(g_{yy} + g_{zz}\right) + k^4 g\right] + O(h^6).\end{aligned} \tag{16}$$

We have from (13) that $g(y, z) = -i\beta u$ and so

$$\begin{aligned}\delta_x u = {} & -i\beta u + \frac{i\beta h^2}{6}\left(u_{yy} + u_{zz} + k^2 u\right) \\ & - \frac{i\beta h^4}{120}\left[u_{yyyy} + 2u_{yyzz} + u_{zzzz} + 2k^2\left(u_{yy} + u_{zz}\right) + k^4 u\right] + O(h^6).\end{aligned} \tag{17}$$

Differentiating (1) twice with respect to y and separately with respect to z and adding we get

$$u_{xxyy} + u_{xxzz} + u_{yyyy} + 2u_{yyzz} + u_{zzzz} + k^2(u_{yy} + u_{zz}) = 0.$$

Substituting this and (1) into (17) we get

$$\begin{aligned}\delta_x u &= -i\beta u - \frac{i\beta h^2}{6}u_{xx} + \frac{i\beta h^4}{120}\left[u_{xxyy} + u_{xxzz} - k^2\left(u_{yy} + u_{zz} + k^2 u\right)\right] + O(h^6)\\ &= -i\beta u - \frac{i\beta h^2}{6}\left(1 - \frac{k^2h^2}{20}\right)u_{xx} + \frac{i\beta h^4}{120}\left(u_{xxyy} + u_{xxzz}\right) + O(h^6).\end{aligned} \tag{18}$$

To approximate (13) to sixth order accuracy we need to approximate u_{xx} to fourth order accuracy and the h^4 term to second order accuracy. Replacing the derivatives in (18) by differences and using (10b) yields a sixth order approximation to (13)

$$\delta_x u = -i\beta u - \frac{i\beta h^2}{6}\left(1 - \frac{k^2h^2}{20}\right)\left[\left(1 + \frac{k^2h^2}{12}\right)\delta_{xx}u + \frac{h^2}{12}(\delta_{xxyy}u + \delta_{xxzz}u)\right] + \frac{i\beta h^4}{120}\left(\delta_{xxyy}u + \delta_{xxzz}u\right) + O(h^6).$$

Simplifying we have the compact approximation to EM1

$$\delta_x u = -i\beta u - \frac{i\beta h^2}{6}\left(1 - \frac{k^2h^2}{30}\right)\delta_{xx}u - \frac{i\beta h^4}{180}\left(\delta_{xxyy}u + \delta_{xxzz}u\right) + O(h^6). \tag{19}$$

In general we shall choose $\beta = k$.

3.4. EM2 with 4th order accuracy

The 2nd order EM ABC is given by (at $x = 0$):

$$0 = (\frac{\partial}{\partial x} - ik)^2 u = u_{xx} - 2iku_x - k^2 u. \tag{20}$$

Putting (10), with $F = 0$, into the EM2 formula (20) we get

$$\left(1 + \frac{k^2h^2}{12}\right)\delta_{xx}u + \frac{h^2}{12}\left(\delta_{xxyy}u + \delta_{xxzz}u\right) - 2ik\left((1 + \frac{k^2h^2}{6})\delta_x u + \frac{h^2}{6}(\delta_{xyy}u + \delta_{xzz}u)\right) - k^2 u = 0.$$

Multiplying by h^2 and regrouping we get

$$-2ikh(1 + \frac{k^2h^2}{6})h\delta_x u + \left(1 + \frac{k^2h^2}{12}\right)h^2\delta_{xx}u - \frac{2ikh}{6}h^3\left(\delta_{xyy}u + \delta_{xzz}u\right) + \frac{h^4}{12}\left(\delta_{xxyy}u + \delta_{xxzz}u\right) - k^2h^2u = 0. \tag{21}$$

The detailed stencil EM2-4th appears in Appendix B.

3.5. 4th order EM ABC with 2nd order accuracy

The fourth order EM (EM4) ABC is given by (at $x = 0$):

$$0 = (\frac{\partial}{\partial x} - ik)^4 u = u_{xxxx} - 4iku_{xxx} - 6k^2u_{xx} + 4ik^3u_x + k^4u. \tag{22}$$

Differentiating the Helmholtz equation (1) ($F = 0$) we replace (22) by

$$\begin{aligned}0 &= -(u_{xxyy} + u_{xxzz} + k^2u_{xx}) + 4ik(u_{xyy} + u_{xzz} + k^2u_x) - 6k^2u_{xx} + 4ik^3u_x + k^4u\\ &= -(u_{xxyy} + u_{xxzz}) + 4ik(u_{xyy} + u_{xzz}) - 7k^2u_{xx} + 8ik^3u_x + k^4u.\end{aligned}$$

So the fourth order EM ABC with second order accuracy is given by

$$-(\delta_{xxyy} + \delta_{xxzz})u + 4ik(\delta_{xyy} + \delta_{xzz})u - 7k^2\delta_{xx}u + 8ik^3\delta_x u + k^4u = 0. \tag{23}$$

3.6. BGT ABCs with 4th order accuracy

For convenience, we repeat the equations for BGT1 and BGT2:

$$\text{BGT1:}\quad B_1 u \equiv u_{\boldsymbol{r}} + \left(\frac{1}{r} - ik\right)u = 0, \tag{24}$$

$$\text{BGT2:}\quad B_2 u \equiv u_{\boldsymbol{rr}} + \alpha(r)u_{\boldsymbol{r}} + \beta(r)u = 0, \tag{25}$$

where

$$\alpha(r) = \left(\frac{4}{r} - 2ik\right)\quad\text{and}\quad\beta(r) = \left(\frac{2}{r^2} - k^2 - \frac{4ik}{r}\right). \tag{26}$$

We have $u_{\boldsymbol{r}} = au_x + bu_y + cu_z$, where $\boldsymbol{r} = (a, b, c)$ is a unit vector in the radial direction. Using the approximation (10a), we obtain the first order radial derivative by central differences with fourth order accuracy:

$$\begin{aligned}\frac{\partial u}{\partial \boldsymbol{r}} = a&\left[\left(1+\frac{k^2h^2}{6}\right)\delta_x u + \frac{h^2}{6}\left(\delta_{xyy}u + \delta_{xzz}u\right)\right]\\ &+ b\left[\left(1+\frac{k^2h^2}{6}\right)\delta_y u + \frac{h^2}{6}\left(\delta_{xxy}u + \delta_{yzz}u\right)\right]\\ &+ c\left[\left(1+\frac{k^2h^2}{6}\right)\delta_z u + \frac{h^2}{6}\left(\delta_{xxz}u + \delta_{yyz}u\right)\right] + O(h^4).\end{aligned} \tag{27}$$

Similarly, using the approximations (10a), (10b) and (12) in Eq. (27), we get the second order derivative of u in the radial (also gradient) direction with 4th order accuracy:

$$\begin{aligned}\frac{\partial^2 u}{\partial \boldsymbol{r}^2} = a^2&\left[\left(1+\frac{k^2h^2}{12}\right)\delta_{xx}u + \frac{h^2}{12}\left(\delta_{xxyy}u + \delta_{xxzz}u\right)\right]\\ &+ b^2\left[\left(1+\frac{k^2h^2}{12}\right)\delta_{yy}u + \frac{h^2}{12}\left(\delta_{xxyy}u + \delta_{yyzz}u\right)\right]\\ &+ c^2\left[\left(1+\frac{k^2h^2}{12}\right)\delta_{zz}u + \frac{h^2}{12}\left(\delta_{xxzz}u + \delta_{yyzz}u\right)\right]\\ &+ 2ab\left[(1+\frac{k^2h^2}{6})\delta_{xy}u + \frac{h^2}{6}\delta_{xyzz}u\right]\\ &+ 2ac\left[(1+\frac{k^2h^2}{6})\delta_{xz}u + \frac{h^2}{6}\delta_{xyyz}u\right]\\ &+ 2bc\left[(1+\frac{k^2h^2}{6})\delta_{yz}u + \frac{h^2}{6}\delta_{xxyz}u\right] + O(h^4).\end{aligned} \tag{28}$$

From Equations (24) and (27), we get the 4th order approximation to BGT1:

$$\begin{aligned}a&\left[\left(1+\frac{k^2h^2}{6}\right)\delta_x u + \frac{h^2}{6}\left(\delta_{xyy}u + \delta_{xzz}u\right)\right]\\ &+ b\left[\left(1+\frac{k^2h^2}{6}\right)\delta_y u + \frac{h^2}{6}\left(\delta_{xxy}u + \delta_{yzz}u\right)\right]\\ &+ c\left[\left(1+\frac{k^2h^2}{6}\right)\delta_z u + \frac{h^2}{6}\left(\delta_{xxz}u + \delta_{yyz}u\right)\right] - iku + \frac{u}{r} = 0.\end{aligned} \tag{29}$$

The detailed stencil for BGT1-4th appears in Appendix B. The eight corners of the stencil have a zero coefficient and so the stencil for BGT1-4th consists of 19 points. To obtain BGT2 to 4th order accuracy, we take Eq. (25) and replace $u_{\boldsymbol{r}}$ and $u_{\boldsymbol{rr}}$ by the expressions in Equations (27) and (28), respectively. To get the 27-point stencil for BGT2, we first replace terms of the type $\delta_x, \delta_{xy}, \ldots$ by their corresponding finite difference approximations, and then collect terms with the same indices. This is similar to the previous cases, so we omit further details.

4. The gradient method for absorbing boundary conditions

The gradient method (GM) for ABCs is based on the original Sommerfeld radiation condition – Eq. (2), which uses the radial derivative, which is also the derivative in the direction of ∇u. The main idea is that every point p on the boundary is considered as if it absorbs the incoming wave at p by approximating the Sommerfeld condition at p. Thus, p is treated as a singleton, i.e., the general shape of the boundary in the vicinity of p is disregarded. In order to do so, any directional derivative of u at p is taken in the *gradient* direction of u at p. In complex situations, there may be several reflecting objects and several sources in the domain, so the radial direction may be irrelevant. Hence, we use the more general gradient direction. This approach allows us to consider arbitrary convex domains. As mentioned previously, derivatives in the normal direction (as in EM) are discontinuous along the edges, leading to inaccurate results. Our results will show the advantage of the GM approach over the standard EM ABCs.

Formally, the GM for ABCs consists of two rules of application:

1. Any directional derivative of u in the ABC is taken in the gradient direction of u.
2. An ABC with such directional derivatives can be applied to any convex domain, with the source (or sources) in any internal position.

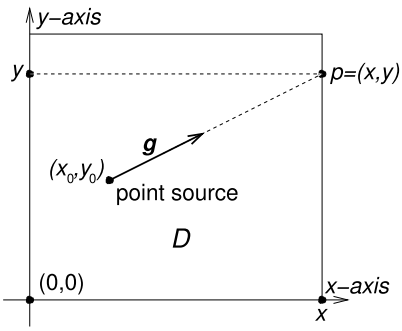

Fig. 1. Domain D with a point source at (x_0, y_0). $\boldsymbol{g}$ is a unit vector in the gradient (also radial) direction towards a point $p = (x, y)$ on the boundary.

If the PDE in question contains several unknown functions, then GM is applied to each of them, even if their gradient directions are different. GM can be used in three different ways:

- The GM can be applied to a known ABC, such as EM, by replacing any derivatives of u with a directional derivative of the same order in the gradient direction of u.
- If some known ABC already uses derivatives in the gradient direction but it is restricted to certain configurations, then it can also be used without these restrictions. The BGT ABCs are examples of this case.
- GM can be used to develop new ABCs using directional derivatives in the gradient direction.

For EM1, GM replaces $u_{\boldsymbol{n}}$ in Eq. (3) by $u_{\boldsymbol{g}}$, where $\boldsymbol{g}$ is a unit vector in the gradient direction of u. The result will be called the "gradient-EM1 ABC", or GEM1 for short:

$$\text{GEM1:}\quad u_{\boldsymbol{g}} - iku = 0. \tag{30}$$

As an example of how $u_{\boldsymbol{g}}$ is calculated, consider the two dimensional case illustrated in Fig. 1 for a square domain D with a point source at (x_0, y_0). Let $p = (x, y)$ be a point on a boundary of D, and denote by r the distance between p and the source, i.e., $r = \sqrt{(x - x_0)^2 + (y - y_0)^2}$. Then the unit vector $\boldsymbol{g}$ in the gradient direction towards p (radial derivative) is $\boldsymbol{g} = \frac{1}{r}(x - x_0, y - y_0)$. For convenience, we denote $a = (x - x_0)/r$ and $b = (y - y_0)/r$, so $\boldsymbol{g} = (a, b)$. Then, the directional derivative of u in the direction of $\boldsymbol{g}$ is

$$\frac{\partial u}{\partial \boldsymbol{g}} = \nabla u \bullet \boldsymbol{g} = au_x + bu_y + cu_z. \tag{31}$$

To calculate $u_{\boldsymbol{gg}}$, we use Eq. (31) with $u_{\boldsymbol{g}}$ in place of u, and we get $u_{\boldsymbol{gg}} = au_{\boldsymbol{g}x} + bu_{\boldsymbol{g}y} + cu_{\boldsymbol{g}z}$. The terms $u_{\boldsymbol{g}x}$, $u_{\boldsymbol{g}y}$, $u_{\boldsymbol{g}z}$ are also obtained from Eq. (31) with u_x, u_y, u_z in place of u. This yields

$$u_{\boldsymbol{gg}} = a^2u_{xx} + b^2u_{yy} + c^2u_{zz} + 2abu_{xy} + 2acu_{xz} + 2bcu_{yz}. \tag{32}$$

This can be continued to any required level of the directional derivatives of u.

The gradient version of EM2 (Eq. (4)), denoted GEM2, is

$$\text{GEM2:}\quad u_{\boldsymbol{gg}} - 2iku_{\boldsymbol{g}} - k^2u = 0, \tag{33}$$

where $u_{\boldsymbol{gg}}$ and $u_{\boldsymbol{g}}$ are obtained from Equations (31) and (32).

In the case of a point source, $u_{\boldsymbol{g}}$ is identical to $u_{\boldsymbol{r}}$ of Eq. (24) of BGT. Using the same notations as above, we can represent BGT1 in Cartesian coordinates as follows

$$au_x + bu_y + cu_z + \left(\frac{1}{r} - ik\right)u = 0. \tag{34}$$

BGT2 can be similarly represented in Cartesian coordinates by using the above expressions for $u_{\boldsymbol{g}}$ and $u_{\boldsymbol{gg}}$. Note that there is no actual change in the BGT equations (as is the case for EM); the application of GM to BGT means that BGT is not restricted to spherical domains with an impact at the center. BGT has been generalized to ellipsoidal and prolate-spheroidal domains based on expansions in Mathieu functions; see [3,4,24,25] and the references therein. However, based on GM, BGT can also be used on box-shaped domains, even with an off-center impact. We shall see that the BGT ABCs produce very good results in such cases.

It is interesting to note that if we take the BGT1 and BGT2 expressions, and allow $r \to \infty$, then we get GEM1 and GEM2, respectively. The coefficients of the unit vector $\boldsymbol{g} = (a, b, c)$ do not vanish as $r \to \infty$, even though r appears in their denominator, because $\boldsymbol{g}$ remains the unit vector in the gradient direction. Hence, the GEM ABCs can be viewed as a special (limit) case of the BGT ABCs. This property is useful in practice: once we have the BGT1 and BGT2 stencils, we get the stencils for GEM1 and GEM2 by replacing $1/r$ and $1/r^2$ by zero.

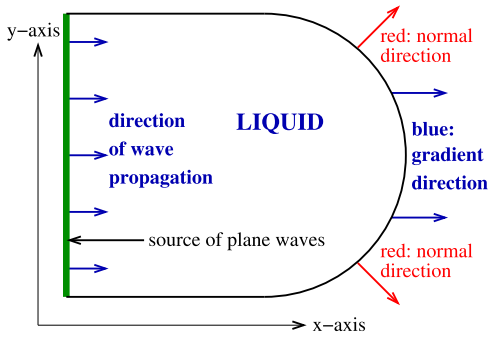

Fig. 2. A ripple tank with plane waves traveling to the right. (For interpretation of the colors in this figure, the reader is referred to the web version of this article.)

GM is not necessarily restricted to waves with a point source. Consider, for example, plane waves in two dimensions. One example is that of a ripple tank [28] with a circular boundary on the right, as illustrated in Fig. 2. A linear paddle on the left creates plane waves traveling to the right, so the gradient direction is just $\boldsymbol{g} = (1, 0)$. This means that in all applications of GM, the directional derivatives will be u_x, u_{xx}, etc. We can see how the normal directions (shown in red) deviate from the gradient direction (blue), except at the center.

In the above examples, the unit vector $\boldsymbol{g}$ (the gradient direction) is known at every boundary point p, so $u_{\boldsymbol{g}}$ can be expressed as a linear combination of u_x, u_y, u_z, with coefficients depending on the coordinates of p. However, this may not always be the case, e.g., when there are one or more scatterers in the domain. We will now consider how this problem may be approached.

The unit vector $\boldsymbol{g}$ in the gradient direction is $\boldsymbol{g} = \nabla u / \|\nabla u\|$, so

$$u_{\boldsymbol{g}} = \nabla u \bullet \boldsymbol{g} = \frac{u_x^2 + u_y^2 + u_z^2}{\sqrt{u_x^2 + u_y^2 + u_z^2}} = \sqrt{u_x^2 + u_y^2 + u_z^2}. \tag{35}$$

To calculate $u_{\boldsymbol{gg}}$, we note first that

$$u_{\boldsymbol{g}x} = \frac{u_x u_{xx} + u_y u_{yx} + u_z u_{zx}}{\sqrt{u_x^2 + u_y^2 + u_z^2}},$$

with similar expressions for $u_{\boldsymbol{g}y}$ and $u_{\boldsymbol{g}z}$. We now use Eq. (35) with $u_{\boldsymbol{g}}$ in place of u and get

$$\begin{aligned} u_{\boldsymbol{gg}} &= \nabla(u_{\boldsymbol{g}}) \bullet \boldsymbol{g} = (u_{\boldsymbol{g}x}, u_{\boldsymbol{g}y}, u_{\boldsymbol{g}z}) \bullet \frac{\nabla u}{\|\nabla u\|} \\ &= \frac{u_x^2 u_{xx} + u_y^2 u_{yy} + u_z^2 u_{zz} + 2(u_x u_y u_{xy} + u_x u_z u_{xz} + u_y u_z u_{yz})}{u_x^2 + u_y^2 + u_z^2}. \end{aligned} \tag{36}$$

Derivatives in the x, y, z directions can be approximated by finite differences, but the expressions for $u_{\boldsymbol{g}}$ and $u_{\boldsymbol{gg}}$ in Equations (35) and (36) lead to non-linear equations. There are several computational methods for dealing with such problems, and we outline here one potentially useful quasi-linear approach:

Algorithm for unknown gradient of u:

- Choose some point s in the domain as a virtual point source of impact.
- Set up the boundary conditions as if the gradient direction of u points away from s.
- **repeat**
  - Solve the resulting linear system until the relative residual falls below some specified threshold t_1.
  - For every boundary point p (of the original grid), calculate numerically new values for $u_{\boldsymbol{g}}$ and $u_{\boldsymbol{gg}}$ using the computed values of u in the neighborhood of p.
  - Modify the equations for the boundary conditions according to the new values of $u_{\boldsymbol{g}}$ and $u_{\boldsymbol{gg}}$.
- **until** the relative difference between two consecutive values of $u_{\boldsymbol{g}}$ (and/or $u_{\boldsymbol{gg}}$) at the boundary points falls below some specified threshold t_2.
- **comment:** Denote by $(p_1, p_2, \ldots)$ the vector of boundary points and let $u_{\boldsymbol{g}}(p_i)$, $u'_{\boldsymbol{g}}(p_i)$ be two consecutive values of $u_{\boldsymbol{g}}$ at p_i. Define two vectors $U = (u_{\boldsymbol{g}}(p_1), u_{\boldsymbol{g}}(p_2), \ldots)$ and $U' = (u'_{\boldsymbol{g}}(p_1), u'_{\boldsymbol{g}}(p_2), \ldots)$, then the relative difference between them is $\frac{\|U - U'\|}{\|U\|}$.
- Continue iterations on the final system of equations until some stopping criterion is satisfied.

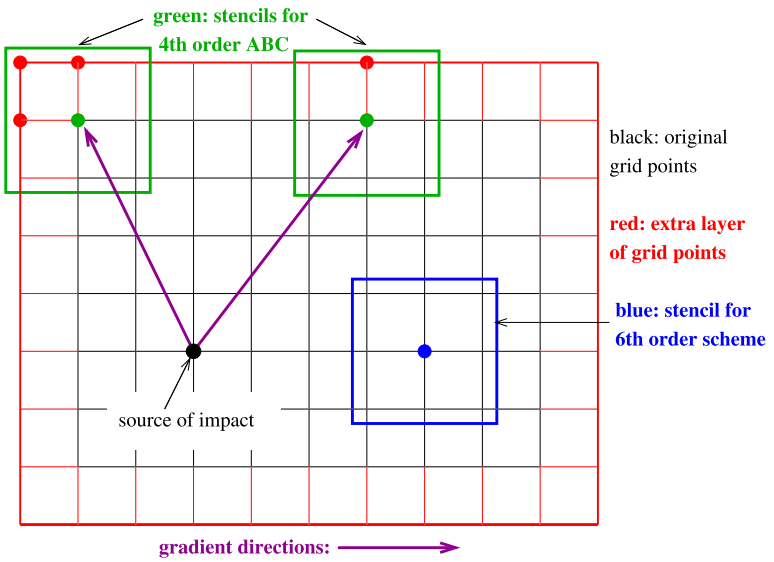

Fig. 3. Explanation (in 2D) of the implementation of the 4th order ABCs. (For interpretation of the colors in this figure, the reader is referred to the web version of this article.)

The initial point s is needed to start the procedure and to ensure that the initial gradient direction is continuous across the entire boundary. It can be taken as the source of impact, or as the center of the scatterer (if there is only one), or simply as the center point of the domain. The calculations and modifications in the inner loop are only done on the small set of boundary points, so they do not impose a heavy computational burden. Furthermore, after the first solve step of the inner loop, every consecutive solve step can start with the values of u from the previous step. The above method can be implemented with GEM1 or GEM2. It is not clear if BGT can be used in all cases because it requires the value of r, and there may be several scatterers which complicate matters. If there is just one unknown source (and no scatterers), then its position can be calculated approximately after the inner loop from the gradient directions of u. BGT can then be used in the final step.

The problem of an unknown gradient direction at the boundaries deserves further study, since it could be useful for complex scattering problems or heterogeneous domains. Nevertheless, we stress here that GM consists of using derivatives in the gradient direction in ABCs on any boundary shape and by any computational means, such as finite differences, finite elements, linear and non-linear computational methods, etc.

5. Implementation details

5.1. Implementation of the ABCs

We first explain how the 4th order ABCs are implemented. To simplify the explanation, this is illustrated for two dimensions in Fig. 3 for a rectangular domain with an internal point source. The original grid is shown in black, and the addition of extra grid points for the ABCs is shown in red. For every original grid point, we have one stencil for the 6th order finite difference scheme of [35] – shown in blue in the figure. This stencil provides one equation, so the number of equations provided by the 6th order scheme is equal to the number of original grid points.

We also need one equation for every one of the additional grid points. These extra equations are supplied by the (green) stencils of the ABC. Consider first the green stencil on the right, centered about a boundary point of the original grid: it provides one equation for the extra grid point marked in red. The gradient direction (which is also the radial direction in this case) points from the source towards the central point of the stencil. For the BGT ABCs, the distance r is measured from the source to the center of the stencil.

In the particular case of high order schemes, a problem arises in the vicinity of corners of two dimensional domains, and also at the corners and also along the edges of three dimensional domains. For 2D, this problem is shown in Fig. 3 at the top left: shown in red are three grid points which have been added for the ABC, together with the (green) stencil containing them. This stencil uses the radial direction and the distance from the point source to the center of the stencil. The result is that if we want to supply exactly one equation for every additional grid point, then we get three identical equations.

In three dimensions we get a multiplicity of equations along the edges and at the corners of box-shaped domains. The existence of identical equations does not cause any problem for our solver (see below), which is based on the Kaczmarz algorithm [21]. Equivalently, we can eliminate the multiple equations. Then there are more unknowns than equations. The Kaczmarz algorithm handles non-square matrices as a least square problem. With the 2nd order ABCs that are based on the

normal (to the boundary) direction, the corner (red) grid point in Fig. 3 is not needed. Furthermore, the two red grid points adjacent to the corner will have different ABC equations because their normals point in different directions. However, as mentioned previously, the deviation of the normals from the gradient direction and their discontinuity at the corners lead to numerical inaccuracies.

An alternative approach to using multiple equations, which we have not pursued in this study, is to consider the equation corresponding to the corner stencil just once as the equation for the extra corner grid point. For each grid point next to the corner, we can add a 4th order equation setting its value as an interpolation between the value of the corner point and a few grid points along the same edge. This approach can be extended to 3D in a straightforward manner. A separate approach to the corner problem has been considered by Bamberger et al. [2].

5.2. The CARP-CG solver

For the solver, we used the block-parallel CARP-CG algorithm [16]. It is simple to implement on structured and unstructured grids, and it is particularly useful for linear systems with large off-diagonal elements, including cases with discontinuous coefficients [15]. At high frequencies, the Helmholtz equation is not positive definite, and the advantage of CARP-CG is that it transforms such systems (even if they are not self-adjoint) into a positive semi-definite, self-adjoint system, to which it applies CG. CARP-CG has been successfully used for high frequency Helmholtz equations [17] with high order schemes from [19,26,30,31,33], but only for constant k in 3D. More recently, this algorithm was used successfully with the new sixth order compact scheme for variable k in Turkel et al. [35].

CARP-CG is based on KACZ – the Kaczmarz algorithm [21], which is actually SOR on the system $AA^*y = b$, $x = A^*y$, where A^* is the conjugate transpose of A. Björck and Elfving [8] showed (in the real case) that by running KACZ in a forward and backward direction, one gets a symmetric positive semi-definite iteration matrix. Their CGMN algorithm is the application of CG to this iteration matrix. Similarly to SOR, KACZ is inherently sequential and requires a relaxation parameter $0 < \lambda < 1$. See [14] for some applications of CGMN to PDEs.

Gordon and Gordon [13] developed a block-parallel version of KACZ, called CARP, which operates as follows: the equations are divided into blocks and then the following two steps are repeated until convergence: (1) KACZ iterations are performed on each block, independently and in parallel. (2) Variables which are common to two or more blocks will now have different values in different blocks, so they are averaged and redistributed. A fundamental property of CARP is that the parallel KACZ operations on the blocks and the averaging operations are equivalent to KACZ iterations in some superspace (but with cyclic relaxation parameters which are not all equal to λ). This property yields an immediate convergence proof for CARP, following [10, Theorem 1.1]. In this work (and in previous studies), CARP was used as a domain decomposition technique in which the averaging equations are done only on variables adjacent to subdomain boundaries, thereby limiting the inter-processor communications to pairs of processors assigned to adjacent subdomains.

Gordon and Gordon extended CGMN to KACZ with cyclic relaxation parameters, and applied it to KACZ in the superspace of the CARP iterations. In the regular space, the result is a CG acceleration of CARP, called CARP-CG [16]. On a single processor, i.e., when all the equations form a single block, CARP-CG is identical to CGMN. It is easy to see that the CARP-CG technique can also be applied to complex systems. On such systems, we have found that it is most efficient run CARP-CG on the real system obtained by interleaving the (real) equations of the real and imaginary parts of the complex system.

We used a relaxation parameter of $\lambda = 1.3$ in all the experiments. There was very little sensitivity to small changes in λ, so we did not try to optimize it. The experiments were done on a Linux cluster with 15 nodes, connected by an Infiniband® network. Each node has a memory of 48 GB and two CPUs, with 6 cores per CPU.

6. Experimental results – problem with an analytic solution

6.1. Evaluation methodology

In this section we present our methodology for comparing the various ABCs. We consider a problem with a constant wave number k and a known analytic solution, and compare the computed results with the analytic solution. The domain D is taken as a three dimensional cube with $0 \le x, y, z \le 1$, with a grid of 169^3 points (168 subintervals on each side). The function F on the RHS of the Helmholtz equation is defined as follows on a cube of size $(2hn_c)^3$ ($n_c >= 1$ is an integer):

$$F(x, y, z) = cos^5\left(\frac{\pi(x - x_0)}{2hn_c}\right) cos^5\left(\frac{\pi(y - y_0}{2hn_c}\right) cos^5\left(\frac{\pi(z - z_0}{2hn_c}\right) /h^2, \tag{37}$$

and zero elsewhere. The cube's center is (x_0, y_0, z_0), and h is the mesh spacing. F is intended to simulate a Dirac delta function, so it has a small support. Some theory for regularizations of a delta function are presented in [40] and [34].

In our experiments, n_c varied from 2 to 12. The division by h^2 in F is just a scaling operation. A one-dimensional version of F is shown in Fig. 4. F and all its derivatives to the 4th order vanish on the sides of the central cube, and they are also zero outside the support of F. The 6th order finite difference scheme of [35] uses the derivatives of F to the 4th order so we need the fourth order derivatives to be continuous in the entire domain.

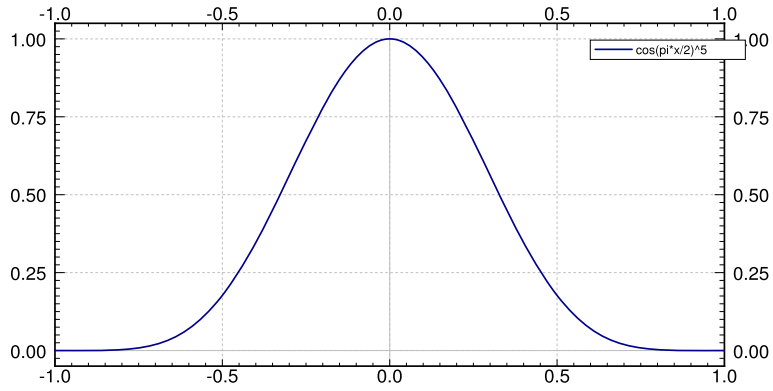

Fig. 4. A plot of $y = \cos^5(\pi x/2)$.

Table 1
Frequencies (f) used in the experiments and the corresponding wave numbers k and number of grid points per wavelength N_g.

f	5	10	20	25
k	31.4	62.8	125.6	157
N_g	33.6	16.8	8.4	6.72

For the n-dimensional Euclidean space, $\mathbb{R}^n$, if the source is at the origin, then the analytic solution to the Helmholtz equation at a point $x \in \mathbb{R}^n$ is

$$u(x) = (G * F)(x) = \int_{\mathbb{R}^n} G(x-y)F(y)dy, \tag{38}$$

where '$*$' denotes the convolution and G is Green's function for dimension n. For $n = 3$,

$$G(x) = \frac{e^{ik\|x\|}}{4\pi\|x\|}. \tag{39}$$

Since F vanishes outside the cube of size $2hn_c^3$, the integral can be easily calculated. In order to get a good approximation, the integral calculation used a subdivision of the cubic support of F that has twice as many subdivision points (in each direction) as the entire domain. To ensure the accuracy of this calculation, we checked the result obtained with an even finer resolution, but there was no significant change.

F is intended to simulate a Dirac delta function of infinitesimally small support, so we compared the computed values of u with the result of the convolution only on points outside the small support of F. Therefore, we avoid a potential problem presented by the denominator in G, which vanishes when $x = y$ in Eq. (38) (the problem is actually only with the real part of $G(x)$, because the imaginary part goes to $k/(4\pi)$ as $\|x\| \to 0$).

In the computations of this section, we used, unless noted otherwise, the 6th order scheme of [35] for variable wave number k. For the boundary conditions, we used the following ABCs: EM1, EM2, GEM2, BGT1 and BGT2. One extra layer of grid points was added to all sides for the boundary conditions, resulting in a grid of 171^3 points. We used the same wave speed, $c = 1$, for all the examples of this section, but we varied the frequency f. The wavelength is calculated as $k = 2\pi f/c$, and the number of grid points per wavelength is $N_g = 2\pi/(kh)$. Table 1 shows the various values of f, k and N_g.

Let u be the calculated solution and u^* be the numerical approximation to the analytic solution, calculated from Eq. (38). The relative error, denoted by rel-err, is calculated as

$$\text{rel-err} = \frac{\|u - u^*\|}{\|u^*\|}.$$

6.2. Experimental results for a simulated delta-like source

The results in this section are all based on the 6th order interior scheme of [35]. Table 2 shows the relative error obtained with various finite difference (FD) schemes and the non-gradient ABCs. The ABCs were also used with different orders of accuracy, as shown in column 2. "p6th-order" stands for the pseudo-6th order of Subsection 3.2. These results are for frequencies $f = 5$, 10, 20, 25, and source at $(0.5, 0.5, 0.5)$. The parameter n_c for the function F of Eq. (37) is chosen as $n_c = 4$, i.e., the support of F is of size $8h \times 8h \times 8h$. We can see that the EM2 ABC with 4th order accuracy, denoted EM2-4th, achieves significantly better results than the others. The pseudo-ABC (15) was not worse than most of the others [36]. Other

Table 2
Relative error results with non-gradient ABCs. The best results are shown in boldface.

FD scheme	ABC & accuracy	$f=5$	$f=10$	$f=20$	$f=25$
2nd order	EM1-2nd order	7.30E−2	1.11E−1	6.54E−1	1.19E 0
6th order [35]	EM1-p6th order	7.20E−2	7.22E−2	6.10E−2	5.46E−2
6th order [35]	EM1-6th order	7.28E−2	7.54E−2	7.36E−2	7.42 E−2
6th order [35]	**EM2-4th order**	**1.13E−2**	**9.77E−3**	**9.37E−3**	**1.10E−2**
6th order [35]	EM4-2nd order	9.10E−2	6.04E−2	3.57E−2	4.20E−2

Table 3
Relative error in different regions of the cube, comparing the best non-gradient ABC, EM2-4th with BGT1-4th. The unit cube was divided into central and corner regions by a sphere of radius 0.5.

ABC	Region	$f=5$	$f=10$	$f=20$	$f=25$
EM2-4th	Central	2.73E−3	2.04E−3	2.68E−3	4.93E−3
	Corner	2.44E−2	2.16E−2	2.03E−2	2.25E−2
BGT1-4th	Central	3.65E−4	2.97E−4	1.70E−3	4.27E−3
	Corner	5.22E−4	3.76E−4	2.09E−3	5.47E−3

Table 4
Relative error comparisons of EM2-4th with its gradient version, GEM2-4th, and with the BGT ABCs with 4th order accuracy. Impact points are at $(0.5, 0.5, 0.5)$ and at $(0.5, 0.5, 0.25)$.

Impact	ABC	$f=5$	$f=10$	$f=20$	$f=25$
At center	EM2-4th	1.13E−2	1.01E−2	9.73E−3	1.15E−2
	GEM2-4th	2.62E−3	6.55E−4	**1.49E−3**	**3.86E−3**
	BGT1-4th	1.73E−4	**2.04E−4**	1.78E−3	4.36E−3
	BGT2-4th	**1.65E−4**	**2.38E−4**	**1.57E−3**	**3.91E−3**
Off-center	EM2-4th	2.66E−2	2.50E−2	2.49E−2	2.60E−2
	GEM2-4th	8.37E−3	2.21E−3	2.04E−3	**4.77E−3**
	BGT1-4th	**1.59E−4**	**1.85E−4**	**1.87E−3**	**4.64E−3**
	BGT2-4th	1.78E−4	2.53E−4	**1.87E−3**	**4.68E−3**

values of n_c produced very similar results to those shown in the table. In view of this, we shall henceforth consider only EM2-4th from among all the non-gradient ABCs.

The normal, to the boundary, derivative of u varies significantly from the gradient direction in the vicinity of the corners. We claim that this is a major source of computational errors when using the EM ABCs. In order to test this hypothesis experimentally, we took the best non-gradient ABC (EM2-4th) and calculated the error over two regions of the unit cube: a central region excluding the corner neighborhoods, and the corner neighborhoods. The central region was taken as the interior of the maximal sphere enclosed by the domain: $(x-0.5)^2+(y-0.5)^2+(z-0.5)^2=0.25$. The corner neighborhoods were taken as the complement of the sphere. Table 3 shows the relative errors for the four frequencies $f=5,10,20,25$, with $n_c=4$ and the source at the center. We see that there is approximately one order of magnitude difference between the results in the central and corner regions, which justifies our hypothesis. For comparison, we also included the results with the BGT1-4th ABC. We see that the differences between the two regions for this ABC are minor when compared to EM2-4th.

In Table 4 we compare four ABCs: EM2-4th (the best non-gradient ABC), GEM2-4th, which is the gradient version of EM2-4th and BGT1 and BGT2, both with 4th order accuracy. In this experiment, $n_c=8$. The comparisons were done with the impact at the center and at an off-center point – $(0.5, 0.5, 0.25)$. The best results are displayed in bold.

The following points can be deduced from Table 4:

- By applying GM to EM2 (GEM2) we get a very significant improvement in accuracy, for both sources of impact.
- On the downside (of GEM2), we can see that if the source is moved closer to a boundary, then GEM2 exhibits a very noticeable drop in accuracy for the lower frequencies.
- The relative error results produced by BGT1 and BGT2 are quite similar to each other. This is not surprising since we have shown that for a Dirac function, they both provide the correct analytic solution on the continuum level.
- For the frequency $f=5$, both BGT1-4th and BGT2-4th are much better than GEM2-4th, but this advantage decreases as the frequency increases.
- Another advantage of BGT1/2 over GEM2-4th is that for any given frequency, they are not sensitive to the position of the source of impact. This difference between GEM2 and BGT1/2 is due to the $1/r$ factors in BGT1 and BGT2.
- The three gradient-based ABCs (GEM2-4th, BGT1-4th and BGT1-4th) achieve fairly similar accuracies with the two higher frequencies. The reason for this is that at high frequencies, the error due to the FD scheme dominates the error due to the ABCs.

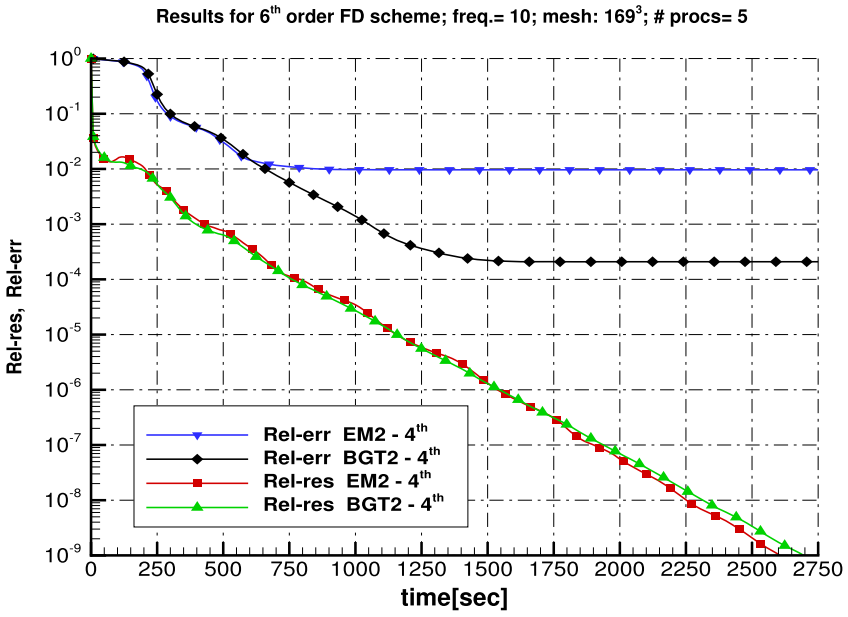

Fig. 5. Relative error and relative residual as a function of time, with the EM2-4th and BGT2-4th ABCs.

It may well be argued that for many practical applications, a relative error of 1% is sufficient and the increased accuracy offered by gradient-based methods is not really important. However, increased accuracy also means that any given relative error objective can also be achieved in a shorter time. This is explained with the aid of Fig. 5, which shows the relative error and relative residual of EM2-4th and BGT2-4th. The advantage of BGT2 is clear, but if a relative error goal of 1% is set, then we can see that EM2 reaches this goal in about 900 seconds. However, by using a smaller grid of size 53^3, BGT2-4th reaches a 1% relative error in only five seconds, which is 0.56% of the time taken by EM2-th. The run times were done on five cores.

Fig. 5 also shows that while the relative error does not improve after a certain point, the relative residual continues to decrease. The reason for this is that the solver continues to improve the relative residual of the given linear system, but the achievable relative error is bound from below not only by the accuracy of the solver, but also by three other factors: the mesh resolution, the accuracy of the FD scheme, and the accuracy of the ABC methods. If a greater accuracy is desired, it would be necessary to refine the mesh.

6.3. Computational results with exact delta and derivative source functions

For many applications, especially in geophysics, one is interested in the situation that the forcing function is a point impact function. We wish to study the efficacy of our various ABC schemes for this case. The point impact function can be modeled by a Dirac delta function or its derivative. However, a delta function cannot be directly simulated in a finite difference setting. Instead, above we modeled the delta function by using an approximation to the delta function (37). This gets increasingly difficult for derivatives of the delta function. Hence, we introduce a different method for comparing our computed solution with the theoretical one. Instead of calculating a convolution integral as before, we assume that the impact point is infinitesimally small, and we have an exact analytic solution. For the constant coefficient Helmholtz equation when the forcing function is the Dirac delta function the solution is the Green's function $G(x, y, z)$ – see Eq. (39). By linearity, when the source is a derivative of the delta function then the solution is the corresponding derivative of the Green's function. In Section 2.3 we have noted that BGT1 is exact when the solution is the Green's function (i.e., the source is a delta function). BGT2 is also exact when the solution is the first derivative of the Green's function (i.e. the source is the first derivative of the delta function). When the source is a second derivative of the delta function it is also known as a Ricker wavelet or a Mexican hat. In this case neither BGT1 nor BGT2 are exact.

We surround the impact point with a small cubic "cage" of size $2n_ch \times 2n_ch \times 2n_ch$, and set the boundary points of the cage equal to the values of the analytic solution. In other words, we impose Dirichlet boundary conditions on the cage's boundary. On the external boundary of the unit cube, we apply our ABC boundary conditions. We also used this method with the original impact function F (Eq. (37)), and the results were very similar to those obtained in Section 6.2.

Table 5 shows the relative error when the solution is G_x, with two locations for the source – at the center and at an off-center point $(0.25, 0.25, 0.25)$. Table 6 shows the results for G_{xx}. For the frequency $f = 25$ we have also added results for a grid of 253^3 points (not including the extra boundary points), so $N_g = 10.08$.

Table 5
Relative error results for the F_1 impact function, when the solution is $G_x(x, y, z)$. Impact points are at $(0.5, 0.5, 0.5)$ and at $(0.25, 0.25, 0.25)$.

Impact	ABC	$f = 5$ $N_g = 33.6$	$f = 10$ $N_g = 16.8$	$f = 20$ $N_g = 8.4$	$f = 25$ $N_g = 6.72$	$f = 25$ $N_g = 10.08$
At center	EM2-4th	1.09E−2	9.22E−3	9.76E−3	1.09E−2	9.00E−3
	GEM2-4th	2.60E−3	6.33E−4	1.48E−3	3.91E−3	6.99E−4
	BGT1-4th	2.10E−3	6.56E−4	1.89E−3	4.63E−3	9.26E−4
	BGT2-4th	2.18E−4	2.20E−4	1.55E−3	3.96E−3	7.46E−4
Off-center	EM2-4th	7.70E−2	5.35E−2	5.22E−2	5.22E−2	5.15E−2
	GEM2-4th	2.58E−2	4.50E−3	5.72E−3	1.32E−2	3.10E−3
	BGT1-4th	7.36E−3	2.04E−3	2.65E−3	5.98E−3	1.33E−3
	BGT2-4th	9.09E−3	3.90E−4	5.36E−3	1.28E−2	2.90E−3

Table 6
Relative error results for the F_2 impact function, when the solution is $G_{xx}(x, y, z)$. Impact points are at $(0.5, 0.5, 0.5)$ and at $(0.25, 0.25, 0.25)$.

Impact	ABC	$f = 5$ $N_g = 33.6$	$f = 10$ $N_g = 16.8$	$f = 20$ $N_g = 8.4$	$f = 25$ $N_g = 6.72$	$f = 25$ $N_g = 10.08$
At center	EM2-4th	8.64E−3	8.34E−3	8.29E−3	1.02E−2	7.80E−3
	GEM2-4th	2.10E−3	5.92E−4	1.71E−3	4.53E−3	8.15E−4
	BGT1-4th	4.07E−3	1.30E−3	2.32E−3	5.41E−3	1.15E−3
	BGT2-4th	1.10E−4	1.96E−4	1.82E−3	4.59E−3	8.79E−4
Off-center	EM2-4th	5.00E−2	4.81E−2	4.86E−2	4.85E−2	4.75E−2
	GEM2-4th	2.16E−2	3.90E−3	5.87E−3	1.36E−2	2.91E−3
	BGT1-4th	1.31E−2	3.82E−3	3.29E−3	6.72E−3	1.65E−3
	BGT2-4th	5.50E−3	4.00E−4	5.71E−3	1.33E−2	2.86E−3

Some remarks on the results shown in Tables 5 and 6:

- As before, in all cases, GEM2-4th provides much better results than EM2-4th.
- In most cases, the BGT ABCs produce better results than the GEM ABCs, especially when the impact is off-center.
- With some exceptions, BGT2 produces better results than BGT1.
- We have used the same grid for all the computations (except for the last column). Hence, the number of points per wavelength decreases as the frequency f increases.
- The last column is also at frequency $f = 25$, but with a larger value of N_g. With the non-gradient ABC (EM2-4th), the larger value of N_g has almost no effect on the accuracy. We can only conclude that for $f = 25$, the error with EM2-4th is mainly due to the inaccuracy of the ABC. With the three gradient-based ABCs, there is a significant increase in accuracy for $f = 25$ when N_g is increased.

7. Experimental results – the SEG/EAGE Salt model

Now we consider the SEG/EAGE Salt model [29], which serves as one of the standard models for geophysics. CARP-CG has previously been used on this specific model [37], and has found other uses in geophysics applications [38], including the frequency domain elastic wave equation [23,27]. The Salt model provides the speed of sound in a 3-dimensional volume of the earth, measuring $13{,}440 \times 13{,}440 \times 4160$ meters^3. The x and y axes are along the longer sides (laid out on the surface), and the z axis goes vertically downwards. There are four variants of this model, discretized at 20, 40, 80, and 160 meters. We studied the 80 meter model, referred to as "model #2", with mesh spacing $h = 80$. The grid size was $169 \times 169 \times 53$, but with the extra grid points for the boundary conditions, it was $171 \times 171 \times 55$. The RHS for the Helmholtz equation was the simulated delta function given by Eq. (37), with $n_c = 8$.

The Salt model is very heterogeneous, with the speed of sound varying from 1500 to 4482 m/s. The relation between the (non-dimensional) wave number k and the speed of sound c is $k = 2\pi f L/c$, where f is the frequency and L is the length of the longest side of the domain. The wavelength is $\lambda = c/f$, and the number of grid points per wavelength is $N_g = \lambda/h$. We set $f = 3.75$, so k, λ and N_g varied as follows: $71 \le k \le 211$, $400 \le \lambda \le 1195$, $5 \le N_g \le 14.94$. Since there is no analytic solution, iterations were ran until a relative residual of 10^{-12} was obtained. Tests were done with the following FD schemes and ABC combinations:

1. The standard 2nd order FD scheme for the original grid points, together with the EM1 ABC with 2nd order accuracy (denoted EM1-2nd).
2. The 6th order compact finite difference scheme of [35] for variable k, together with the EM2 ABC with 4th order accuracy (denoted EM2-4th).
3. The same finite difference scheme as in 2, together with the BGT1 ABC with 4th order accuracy (denoted BGT1-4th).

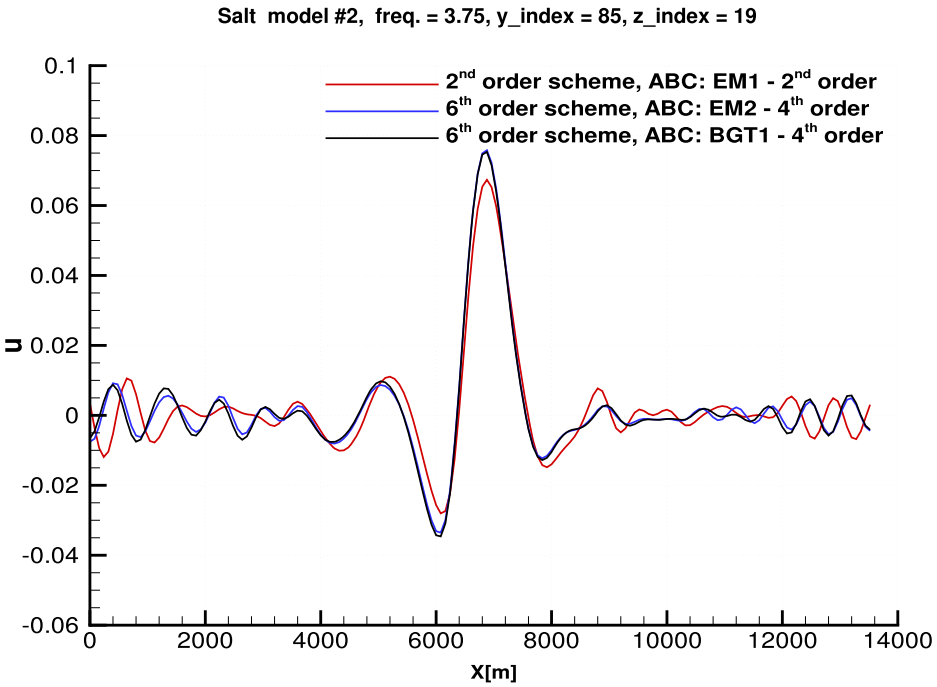

Fig. 6. Plot of the Salt model, with $y = 85$ and $z = 19$: close to the center of the domain. The plots are all quite close to each other at the center, but EM1-2nd deviates significantly towards the two sides, ending in opposite amplitudes with respect to the other two.

4. In addition, two plots with the same finite difference scheme as in 2, with four ABCs: EM2-4th, GEM2-4th, BGT1-4th and BGT2-4th.

The following four figures plot the values of u against the x-axis, along a single line of constant y and z values, with $0 \le y \le 169$ and $0 \le z \le 53$. In these plots, the value of x is measured in meters, i.e., $0 \le x \le 13,440$. The figure captions provide additional details and comments.

Fig. 6 shows plots close to a line through the center of the domain. The plots indicate that all the tested methods are in good agreement in the central region of the domain. However, towards the boundaries, the results of the second order FD scheme with the EM1-2nd ABC deviate very significantly from the results of the high order schemes. This result is also corroborated by the plots of Fig. 7. Thus, we now drop the second order FD scheme and the EM1-2nd ABC from further consideration.

Fig. 7, which is close to the side of the domain, also shows that the non-gradient EM2-4th ABC varies significantly from BGT1-4th in the central region, though it is still not clear from this figure which of the two is more accurate. But now, Fig. 8 shows plots that are close to an edge of the domain. These plots indicate that the two gradient-based ABCs, GEM2-4th and BGT2-4th are almost identical, and BGT1-4th is quite close to them, so we can surmise that BGT1-4th is more accurate than EM2-4th ABC. This figure also shows that the only non-gradient ABC, EM2-4th, deviates from the three quite significantly.

Fig. 9 shows plots of the same ABCs as those of Fig. 8, but here, the plots are close to a side of the domain (but not close to an edge). Again, we see that the three gradient-direction based ABC produce fairly similar plots, while the non-gradient ABC (EM2-4th) is markedly different. Furthermore, similarly to the previous results, the two fourth order gradient direction ABCs, GEM2-4th and BGT2-4th are almost identical.

The conclusion is that the gradient-direction based ABCs are significantly more accurate than the non-gradient ABCs. From among the gradient-based ABCs, the higher order ones – GEM2-4th and BGT2-4th – are almost identical, so we can presume that they are more accurate than GEM1-4th and BGT1-4th. These conclusions are in agreement with the results with a known analytic solution.

8. Conclusions

We have developed accurate compact absorbing boundary conditions (ABCs) for the Helmholtz equation, based on two complementary approaches: compact high order approximation to two ABC schemes, and a new “gradient-direction method” (GM) for ABCs. The compact high order schemes are based on two methods: the Engquist–Majda (EM) ABC [11] and the Bayliss, Gunzburger and Turkel (BGT) ABC [5]. GM consists of using directional derivatives in an ABC scheme in the direction of the gradient of the unknown function $u(x, y, z)$. The BGT ABCs are already based on such directional derivatives, but they

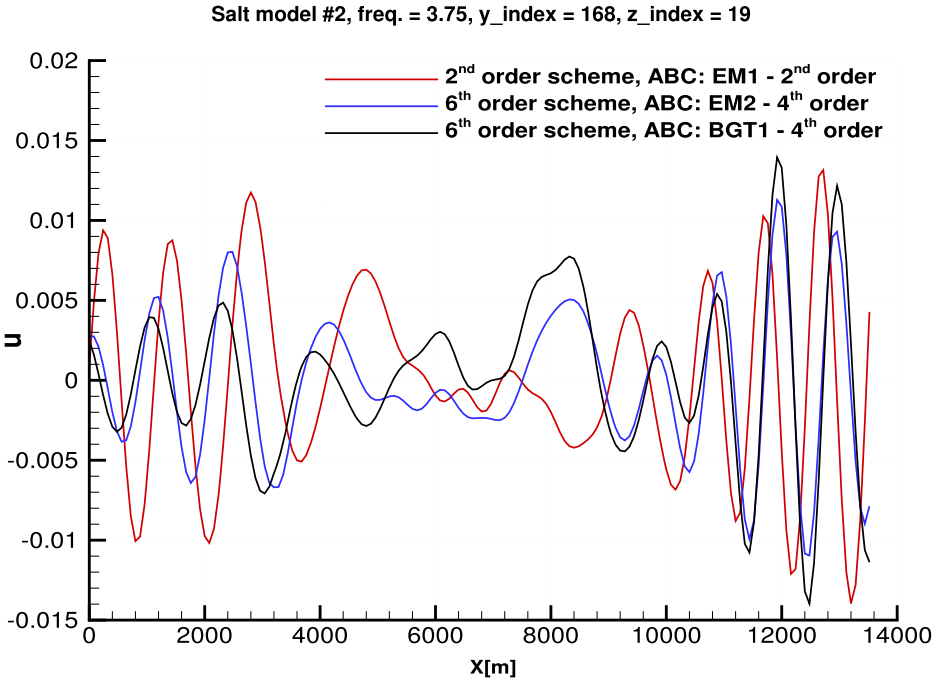

Fig. 7. Plot of the Salt model, with $y = 168$ and $z = 19$: close to a side of the domain. EM1-2nd deviates widely from the other two, and EM2-4th and BGT1-4th vary significantly in the center region.

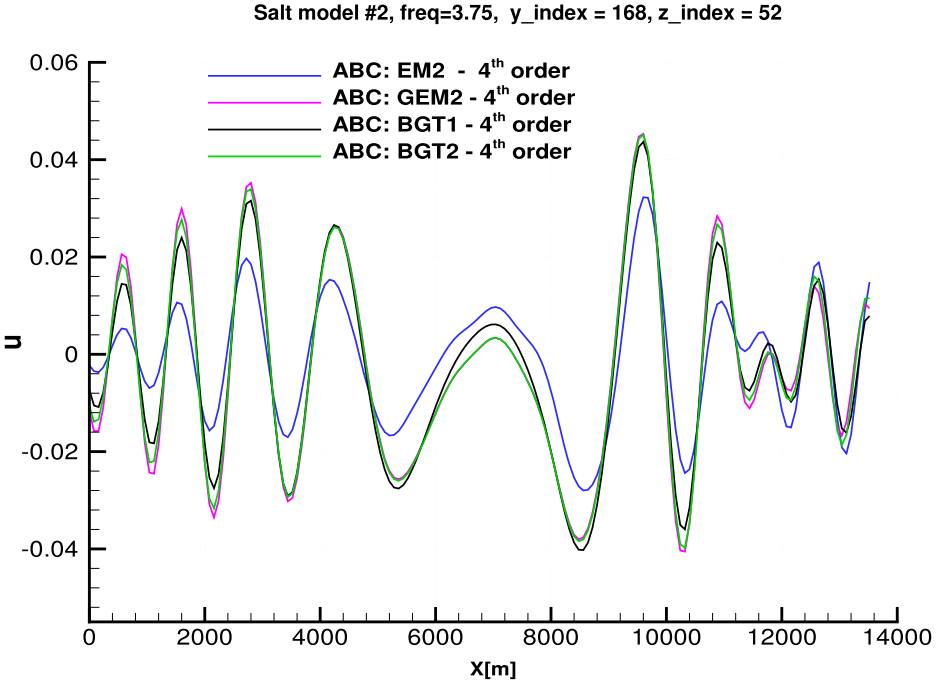

Fig. 8. Plot of the Salt model, with $y = 168$ and $z = 52$: close to an edge of the domain. EM2-4th deviates significantly from the others, and GEM2-4th and BGT2-4th are almost indistinguishable.

were originally restricted to certain configurations; the application of GM to the BGT ABCs means that these restrictions can be removed. If we have a radial source then we can assume a priori that the gradient direction is in the radial direction.

Experiments on problems with known analytic solutions demonstrate that the best EM scheme is the second order one with fourth order accuracy. We also show that the error in using the EM ABCs is concentrated mainly in the corner regions (this was the motivation for GM). We then apply GM to the EM ABCs by changing the derivatives normal to the boundary

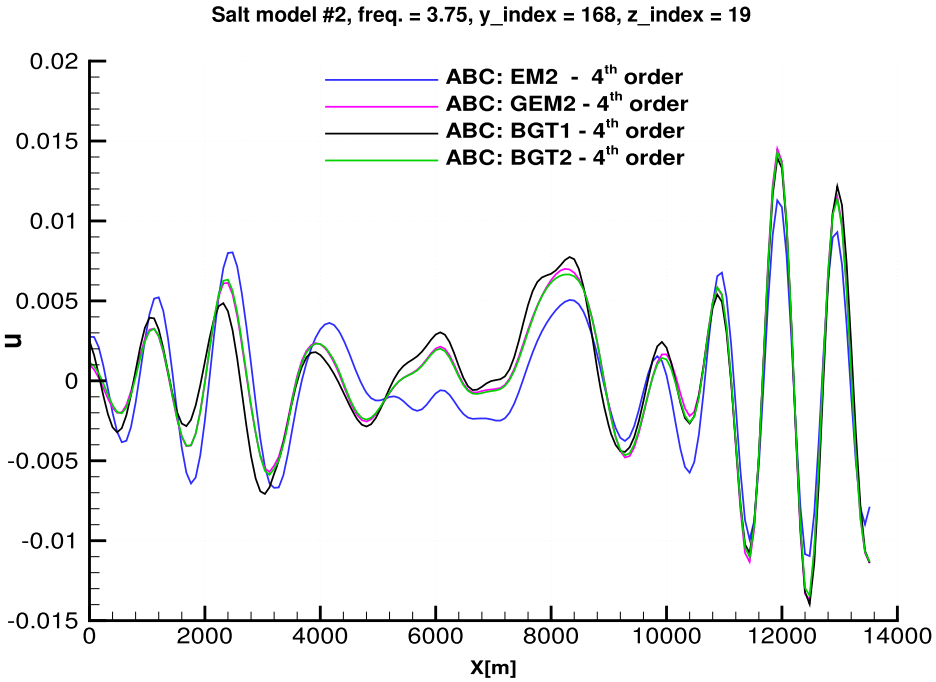

Fig. 9. Plot of the Salt model, with $y = 168$ and $z = 19$: close to a side of the domain. EM2-4th deviates very significantly from the others, especially in the central region. Similarly to Fig. 8, GEM2-4th and BGT2-4th are almost indistinguishable.

to derivatives in the gradient direction; we called these schemes GEM. GEM is shown to significantly decrease the overall error of EM. Comparisons between the GEM and BGT ABCs show that generally, the BGT ABCs are better, especially in cases where the source of impact is off-center. BGT1 and BGT2 produced similar results for a simulated delta source, but when the source was a wavelet function, then BGT2 was better in most of the cases.

Experiments on the SEG/EAGE Salt model [29] show a very good agreement between the GEM and BGT high order ABCs. However, the EM ABCs produced very wayward results, except at the very center of the domain (which was also the point source of impact).

Future research in this direction is expected to continue in two main directions: high order gradient-based ABCs for other equations, and also the application of GM to complex scattering problems, where the gradient of the unknown function is not known a priori.

Acknowledgements

The authors wish to thank Semyon Tsynkov for his valuable comments. Thanks are also due to the anonymous reviewers for their helpful comments.

Appendix A. Self-adjointness of ABCs for Helmholtz equation

The Helmholtz equation, by itself, is easily seen to be a symmetric/self-adjoint equation. For high frequencies however, it is not positive definite. Hence, simple iterative methods like conjugate-gradient do not work. For an interior problem one needs to use an iterative method that works for self-adjoint but non-positive-definite problems.

For an exterior problem one needs to impose the Sommerfeld radiation condition for the continuous case and some ABC for the discrete problem. One can easily verify that the Sommerfeld radiation condition destroys the self-adjointness of the entire system. We shall now investigate whether the various ABCs we consider preserve the self-adjointness of the system or not. If the system, including the ABC, remains self-adjoint then one can use an iterative method applicable for self-adjoint but non-positive-definite systems. If the ABC destroys the self-adjointness of the total matrix then one must use a more general iterative method.

In addition to the practical aspect it is interesting to see whether one can approximate the non-self-adjoint system using the Sommerfeld radiation condition, with a symmetric (self-adjoint) matrix. This can effect the stability of the system. For the time dependent wave equation this has been investigated in [1].

We shall now consider both the continuous and discrete cases with various order EM ABCs.

A.1. Continuous equation

Consider the two dimensional equation

$$Lu = -\left(\frac{\partial^2 u}{\partial x^2} + \frac{\partial^2 u}{\partial y^2}\right) - k^2 u = 0 \quad 0 \le x, y \le 1, \tag{40a}$$

$$u(0, y) = 0 \quad 0 \le x \le 1, \qquad u(1, y) \text{ satisfies an ABC}, \tag{40b}$$

$$u(x, 0) = u(x, 1) = 0 \quad 0 \le y \le 1. \tag{40c}$$

For simplicity we first consider the first order Engquist–Majda EM1 ABC:

$$\frac{\partial u}{\partial x} - iku = \frac{1}{i}\left(i\frac{\partial u}{\partial x} + ku\right) = 0 \quad x = 1. \tag{41}$$

We have moved the i from multiplying the ku to multiplying $\frac{\partial u}{\partial x}$ so that $i\frac{\partial u}{\partial x}$ is self-adjoint. Now both the interior PDE and the boundary condition are self-adjoint considered separately. The question we consider is whether the combined PDE-BC problem is self-adjoint.

Using the standard Green's formula, with a test function v satisfying $\frac{\partial v}{\partial x} - ikv = 0$ we have

$$\begin{aligned}(Lu, v) - (u, Lv) &= \int \left(\bar{v}\frac{\partial u}{\partial n} - u\frac{\partial \bar{v}}{\partial n}\right) ds \\ &= \int_0^1 \left(\bar{v}\frac{\partial u}{\partial x} - u\frac{\partial \bar{v}}{\partial x}\right)_{x=1} dy \quad \text{using } u = 0 \text{ on 3 sides} \\ &= \int_0^1 (iku\bar{v} + iku\bar{v})\, dy \neq 0 \quad \text{from (41)}.\end{aligned}$$

Thus, for the operator to be self-adjoint the test function v needs to satisfy $\frac{\partial v}{\partial x} + ikv = 0$ at $x = 1$ i.e. to be incoming.

Similarly we can find the eigenvalues by considering $Lu = \lambda u$, multiplying by $\bar{u}$ and integrating. Again using Green's formula we then get

$$\lambda \iint |u|^2 x\, dxdy = \iint \left(|\nabla u|^2 - k^2|u|^2\right) dxdy + \int \bar{u}\frac{\partial u}{\partial n} ds \tag{42a}$$

$$= \iint \left(|\nabla u|^2 - k^2|u|^2\right) dxdy + \int_0^1 \bar{u}\frac{\partial u}{\partial x}|_{x=1}\, dy \tag{42b}$$

$$= \iint \left(|\nabla u|^2 - k^2|u|^2\right) dxdy + ik\int_0^1 |u|^2 dy. \tag{42c}$$

So λ is not real. If we replace the first order EM1 operator by the second order operator we have at $x = 1$

$$\left(\frac{\partial}{\partial x} - ik\right)^2 u = 0$$

or

$$\frac{\partial^2 u}{\partial x^2} - 2ik\frac{\partial u}{\partial x} - k^2 u = 0 \quad \text{at } x = 1. \tag{43}$$

Thus, the second order EM2 operator considered by itself is self-adjoint. We have from (43)

$$\begin{aligned}\frac{\partial u}{\partial x} &= \frac{1}{2ik}\left(\frac{\partial^2 u}{\partial x^2} - k^2 u\right) \quad \text{at } x = 1 \\ &= \frac{1}{2ik}\left(-\frac{\partial^2 u}{\partial y^2} - 2k^2 u\right) \quad \text{from (43)} \\ &= \frac{i}{2k}\left(\frac{\partial^2 u}{\partial y^2} + 2k^2 u\right).\end{aligned} \tag{44}$$

Substituting this into (42b) we get

$$\lambda \iint |u|^2 dxdy = \iint \left(|\nabla u|^2 - k^2|u|^2\right) dxdy + \int_0^1 \bar{u}\frac{\partial u}{\partial x} dy$$

$$= \iint \left(|\nabla u|^2 - k^2|u|^2\right) dxdy + \frac{i}{2k}\int_0^1 \bar{u}\left(\frac{\partial^2 u}{\partial y^2} + 2k^2 u\right) dy$$

$$= \iint \left(|\nabla u|^2 - k^2|u|^2\right) dxdy + \frac{i}{2k}\int_0^1 \left(-|\frac{\partial u}{\partial y}|^2 + 2k^2|u|^2\right) dy$$

and again the eigenvalues are complex.

A.2. Discrete EM absorbing boundary conditions

For a finite element approximation we follow the above procedure and again find that the combined interior + BC operator is not self-adjoint and has complex eigenvalues. The only change from the above analysis is the spaces that the functions occupy.

For a finite difference scheme we replace the interior Helmholtz equation by a standard second order approximation which yields a symmetric matrix. To treat the ABC we add an extra line exterior to $x = 1$, i.e., $i = I + 1$. On the boundary $i = I$ we impose two separate equations. One is the interior Helmholtz equation which is now defined since $i = I + 1$ is in the computational domain. A second equation is a second order centered approximation to the EM ABC. Since we have shown that the EM ABC considered by itself is self-adjoint it implies that the approximation will lead to a self-adjoint matrix.

Therefore, the total matrix approximation including both the interior scheme and the EM ABC will be self-adjoint as opposed to the continuous equation which is not self-adjoint when the EM ABC is used.

Appendix B. Stencils for EM2-4TH and BGT1-4th

For the EM2-4th stencil, we denote the coefficient of u by A. We then have at $i = 0$ and all j (not the corners), in two dimensions, in the 3×3 stencil

$$A_{i+1,j\pm1} = \frac{1}{12} - i\frac{kh}{6}, \qquad A_{i-1,j\pm1} = \frac{1}{12} + i\frac{kh}{6}, \qquad A_{i,j\pm1} = -\frac{1}{6},$$

$$A_{i\pm1,j} = 1 + \frac{k^2h^2}{12} - \frac{1}{6} \pm i\frac{2kh}{6} \mp ikh(1 + \frac{k^2h^2}{6}) = \frac{5}{6} + \frac{k^2h^2}{12} \mp \frac{ikh}{6}(4 + k^2h^2),$$

$$A_{i,j} = \frac{1}{3} - 2(1 + \frac{k^2h^2}{12}) - k^2h^2 = -\frac{5}{3} - \frac{7}{6}k^2h^2.$$

In three dimensions this becomes at $i = 0$ and all j, k:

$$A_{i+1,j\pm1,k} = \frac{1}{12} - i\frac{kh}{6}, \qquad A_{i-1,j\pm1,k} = \frac{1}{12} + i\frac{kh}{6},$$

$$A_{i+1,j,k\pm1} = \frac{1}{12} - i\frac{kh}{6}, \qquad A_{i-1,j,k\pm1} = \frac{1}{12} + i\frac{kh}{6},$$

$$A_{i,j\pm1,k} = -\frac{1}{6}, \qquad A_{i,j,k\pm1} = -\frac{1}{6},$$

$$A_{i\pm1,j,k} = \frac{2}{3} + \frac{k^2h^2}{12} \mp \frac{ikh}{6}(2 + k^2h^2),$$

$$A_{i,j,k} = \frac{2}{3} - 2(1 + \frac{k^2h^2}{12}) - k^2h^2 = -\frac{4}{3} - \frac{7}{6}k^2h^2.$$

The stencil for BGT1-4TH is derived similarly to the stencil for EM2-4th. It is identical for all 6 sides of the domain. There are no cases where all three of i, j, k have ±1 attached to them. This means that the expressions for the eight corners of the $3 \times 3 \times 3$ stencil are all zero, i.e., the stencil consists of 19 points.

$$A_{i,j,k} = \frac{h}{r} - ikh, \qquad A_{i\pm1,j,k} = \pm\frac{a}{6}\left(1 + \frac{k^2h^2}{2}\right),$$

$$A_{i,j\pm1,k} = \pm\frac{b}{6}\left(1+\frac{k^2h^2}{2}\right), \qquad A_{i,j,k\pm1} = \pm\frac{c}{6}\left(1+\frac{k^2h^2}{2}\right),$$
$$A_{i+1,j\pm1,k} = \frac{a\pm b}{12}, \qquad A_{i-1,j\pm1,k} = \frac{-a\pm b}{12},$$
$$A_{i+1,j,k\pm1} = \frac{a\pm c}{12}, \qquad A_{i-1,j,k\pm1} = \frac{-a\pm c}{12},$$
$$A_{i,j+1,k\pm1} = \frac{b\pm c}{12}, \qquad A_{i,j-1,k\pm1} = \frac{-b\pm c}{12}.$$

References

[1] D. Baffet, D. Givoli, On the stability of the high-order Higdon absorbing boundary conditions, Appl. Numer. Math. 61 (2011) 768–784.
[2] A. Bamberger, P. Joly, J.E. Roberts, Second-order absorbing boundary conditions for the wave equation: a solution to the corner problem, SIAM J. Numer. Anal. 27 (2) (1990) 323–352.
[3] H. Barucq, R. Djellouli, A. Saint-Guirons, Performance assessment of a new class of local absorbing boundary conditions for elliptical and prolate-spheroidal shaped boundaries, Appl. Numer. Math. 59 (2009) 1467–1498.
[4] H. Barucq, R. Djellouli, A. Saint-Guirons, Three-dimensional approximate local DtN boundary conditions for prolate spheroid boundaries, J. Comput. Appl. Math. 234 (2010) 1810–1816.
[5] A. Bayliss, M. Gunzburger, E. Turkel, Boundary conditions for the numerical solution of elliptic equations in exterior regions, SIAM J. Appl. Math. 42 (1982) 430–451.
[6] J.-P. Berenger, A perfectly matched layer for the absorption of electromagnetic waves, J. Comput. Phys. 114 (1994) 185–200.
[7] J.-P. Berenger, Three dimensional perfectly matched layer for the absorption of electromagnetic waves, J. Comput. Phys. 127 (1996) 363–379.
[8] Å. Björck, T. Elfving, Accelerated projection methods for computing pseudoinverse solutions of systems of linear equations, BIT 19 (1979) 145–163.
[9] Y.A. Erlangga, E. Turkel, Iterative schemes for high order compact discretizations to the exterior Helmholtz equation, ESAIM: Math. Model. Numer. Anal. 46 (3) (2012) 647–660.
[10] P.P.B. Eggermont, G.T. Herman, A. Lent, Iterative algorithms for large partitioned linear systems, with applications to image reconstruction, Linear Algebra Appl. 40 (1981) 37–67.
[11] B. Engquist, A. Majda, Absorbing boundary conditions for the numerical simulation of waves, Math. Comput. 31 (1977) 629–651.
[12] D. Givoli, High-order local non-reflecting boundary conditions: a review, Wave Motion 39 (4) (2004) 319–326.
[13] D. Gordon, R. Gordon, Component-averaged row projections: a robust, block-parallel scheme for sparse linear systems, SIAM J. Sci. Comput. 27 (2005) 1092–1117.
[14] D. Gordon, R. Gordon, CGMN revisited: robust and efficient solution of stiff linear systems derived from elliptic partial differential equations, ACM Trans. Math. Softw. 35 (3) (2008) 18:1–18:27.
[15] D. Gordon, R. Gordon, Solution methods for linear systems with large off-diagonal elements and discontinuous coefficients, CMES Comput. Model. Eng. Sci. 53 (1) (2009) 23–45.
[16] D. Gordon, R. Gordon, CARP-CG: a robust and efficient parallel solver for linear systems, applied to strongly convection dominated PDEs, Parallel Comput. 36 (2010) 495–515.
[17] D. Gordon, R. Gordon, Parallel solution of high frequency Helmholtz equations using high order finite difference schemes, Appl. Math. Comput. 218 (21) (2012) 10737–10754.
[18] Y. Gryazin, Preconditioned Krylov subspace methods for sixth order compact approximations of the Helmholtz equation, ISRN Comput. Math. 2014 (2014), article ID 745849, 15 pp.
[19] I. Harari, E. Turkel, Accurate finite difference methods for time-harmonic wave propagation, J. Comput. Phys. 119 (2) (1995) 252–270.
[20] R.L. Higdon, Numerical absorbing boundary conditions for the wave equation, Math. Comput. 49 (1987) 65–90.
[21] S. Kaczmarz, Angenäherte auflösung von systemen linearer gleichungen, Bull. Acad. Pol. Sci. Lett. A 35 (1937) 355–357.
[22] G.A. Kriegsmann, A. Taflove, K.R. Umashankar, A new formulation of electromagnetic scattering using on surface radiation condition approach, IEEE Trans. Antennas Propag. AP35 (1987) 153–161.
[23] Y. Li, L. Métivier, R. Brossier, B. Han, J. Virieux, 2D and 3D frequency-domain elastic wave modeling in complex media with a parallel iterative solver, Geophysics 80 (3) (2015) T101–T118.
[24] M. Medvinsky, E. Turkel, U. Hetmaniuk, Local absorbing boundary conditions for elliptical shaped bodies, J. Comput. Phys. 227 (2008) 8254–8267.
[25] M. Medvinsky, E. Turkel, On surface radiation conditions for an ellipse, J. Comput. Appl. Math. 234 (2010) 1647–1655.
[26] M. Nabavi, K. Siddiqui, J. Dargahi, A new 9-point sixth-order accurate compact finite-difference method for the Helmholtz equation, J. Sound Vib. 307 (2007) 972–982.
[27] B. Pajot, Y. Li, V. Berthoumieux, C. Weisbecker, R. Brossier, L. Métevier, P. Thierry, S. Operto, J. Virieux, A review of recent forward problem developments used for frequency-domain FWI, in: Proc. 76th EAGE Conference & Exhibition, Amsterdam, The Netherlands, June 2014.
[28] Ripple Tank, Wikipedia, http://en.wikipedia.org/wiki/Ripple_tank.
[29] SEG/EAGE: 3-dimensional geophysics problems, http://geodus1.ta.tudelft.nl/seage3dm.
[30] I. Singer, E. Turkel, High-order finite difference methods for the Helmholtz equation, Comput. Methods Appl. Mech. Eng. 163 (1–4) (1998) 343–358.
[31] I. Singer, E. Turkel, Sixth order accurate finite difference schemes for the Helmholtz equation, J. Comput. Acoust. 14 (2006) 339–351.
[32] A. Sommerfeld, Partial Differential Equations in Physics, Academic Press, New York, 1964.
[33] G. Sutmann, Compact finite difference schemes of sixth order for the Helmholtz equation, J. Comput. Appl. Math. 203 (1) (2007) 15–31.
[34] A.-K. Tornberg, B. Engquist, Numerical approximations of singular source terms in differential equations, J. Comput. Phys. 200 (2004) 462–488.
[35] E. Turkel, D. Gordon, R. Gordon, S. Tsynkov, Compact 2D and 3D sixth order schemes for the Helmholtz equation with variable wave number, J. Comput. Phys. 232 (1) (2013) 272–287.
[36] E. Turkel, Comments on iterative schemes for high order compact discretizations to the exterior Helmholtz equation, ESAIM: Math. Model. Numer. Anal. 49 (1) (2015) 221–223.
[37] T. van Leeuwen, D. Gordon, R. Gordon, F. Herrmann, Preconditioning the Helmholtz equation via row projections, in: Proc. 74th EAGE Conference, Copenhagen, Denmark, EAGE, June 2012, pp. 60–65.
[38] T. van Leeuwen, F. Herrmann, 3D frequency-domain seismic inversion with controlled sloppiness, SIAM J. Sci. Comput. 36 (5) (2014) S192–S217.
[39] J. Virieux, S. Operto, An overview of full-waveform inversion in exploration geophysics, Geophysics 74 (6) (2009) wcc127–wcc152.
[40] J. Walden, On the approximation of singular source terms in differential equations, Numer. Methods Partial Differ. Equ. 15 (4) (1999) 407–534.
[41] A. Zarmi, E. Turkel, A general approach for high order absorbing boundary conditions for the Helmholtz equation, J. Comput. Phys. 242 (2013) 387–404.